The next generation of mid-IR laser-based refractive index (dispersion) spectroscopy of liquid-phase analytes

Alicja Dabrowska, Andreas Schwaighofer, Bernhard Lendl*
Institute of Chemical Technologies and Analytics, Technische Universität Wien,
Getreidemarkt 9/E164, A-1060 Vienna, Austria

ABSTRACT

Mid-infrared dispersion spectroscopy is a novel alternative approach to classical absorption spectroscopy for qualitative and quantitative analysis of liquid-phase samples focused on broadband refractive index variation sensing originating from IR absorption. We present the redesigned and improved version of an external cavity-quantum cascade laser-based Mach-Zehnder interferometer setup dedicated for refractive index sensing of liquids, which outperforms classic absorption spectroscopy. The refined version of the setup features greater compactness, a new dual-channel transmission cell and a hysteresis-free piezo-actuator for phase locked interferometric detection. Moreover, a new routine for fast and almost simultaneous acquisition of real and imaginary part of the complex refractive index (i.e., dispersion and absorption spectra) was introduced for mutual validation of the spectra. Dispersion spectra at sample temperatures ranging from 15 to 90 °C can be recorded as the setup shows a stable noise-floor over that temperature range. Introduction of a hysteresis-free piezo-actuator to the system enabled fast spectral acquisition at constant sensitivity with speed rates of 100 cm^{-1}/s, long-term stability and allowed to improve the reproducibility, robustness, and limits of detection of the method. We compare the performance of the refined setup with the previously demonstrated version by comparing the figures of merit for univariate glucose detection. In this context, the dispersion and absorption spectra of glucose were acquired and assessed. The achieved limit of detection for dispersion sensing was 5 times lower when compared to previous version and ~2 times lower than for classic absorption sensing at 5 times shorter spectra acquisition times. In summary, the improvements in the instrumentation for dispersion spectroscopy have improved the sensitivity, reliability, and quality of the method. The achieved results set a basis for further extension of the range of application presented for this technique.

Keywords: mid-infrared spectroscopy, quantum cascade lasers, dispersion spectroscopy, refractive index sensing, Mach-Zehnder interferometer, liquid-phase analysis, carbohydrates analysis

The published version of this accepted manuscript is available under: A. Dabrowska, A. Schwaighofer, and B. Lendl, "The next generation of mid-IR laser-based refractive index (dispersion) spectroscopy of liquid-phase analytes," Proc. SPIE 11957, Biomedical Vibrational Spectroscopy 2022: Advances in Research and Industry, 119570D (2 March 2022), DOI: 10.1117/12.2609371

1. INTRODUCTION

Mid-infrared (mid-IR) spectroscopy (400 – 4000 cm^{-1}) is an established and powerful analytical technique allowing for highly selective, sensitive, and non-destructive sample investigation by probing fundamental molecular vibrations.[1] The introduction of quantum cascade lasers (QCLs)[2] offering coherent and polarized mid-IR radiation enabled new spectroscopy schemes that go beyond classical absorption spectroscopy.[3] In this context, dispersion spectroscopy is one alternative technique focused on detection of the refractive index changes of the sample in the vicinity of an absorption band to derive quantitative and qualitative information about the sample. The absorption process leads not only to attenuation of the radiation intensity (absorption spectroscopy) upon passing through a sample but also to a phase shift of the passing light. The light slows down in the absorbing medium introducing changes in the phase velocity proportional to the refractive index of the sample. Hence, the absorbing medium can be described by a complex refractive index function, where the imaginary part $\kappa(\tilde{\nu})$, known as absorption index is responsible for the exponential decay in intensity of light and the real part $n(\tilde{\nu})$ accounts for the phase velocity and is known as refractive index. Both properties are analyte-specific and are interrelated via the Kramers-Kronig transformation (KKT). Due to dispersion, the refractive index of the absorbing materials is not a constant value. For regions far from the absorption band, the change of the refractive index is

very slow and shows positive slope with increasing wavenumber ($\partial n/\partial \tilde{\nu}$>0, normal dispersion), whereas in the proximity to the absorption band (peak of imaginary part of the complex refractive index), the real part of the complex refractive index will exhibit a rapid negative change ($\partial n/\partial \tilde{\nu}$>0, anomalous dispersion).[4] The distinct regions of anomalous dispersion can be analyzed to derive information about of the sample. Hence, dispersion (phase shift) sensing delivers quantitative and qualitative information about the sample equivalent to absorption spectroscopy with the advantages of: (i) immunity to source intensity fluctuations associated with high-intensity laser sources, (ii) extended dynamic range for quantitative analysis, (iii) constant sensitivity, and (iv) baseline-free detection.[5] Current implementations of mid-IR dispersion spectroscopy are based on coherent laser sources (QCLs) and interferometric detection. While QCL-based dispersion spectroscopy of gaseous samples is an established technique,[5–7] it is still an emerging approach for liquid-phase samples. So far, proof-of-concept setups employing an external cavity QCL (EC-QCL) integrated in a Mach-Zehnder interferometer (MZI) were reported.[8,9] For liquid-phase measurements, EC-QCLs are preferable since they provide large spectral coverage (typically over 200 cm^{-1}) allowing broadband investigation of liquid-phase absorptions. Most recently, the EC-QCL-MZI setup featuring low-noise and higher reproducibility due to enhanced acquisition rates and temperature control was used to demonstrate protein detection with dispersion spectroscopy.[10] Despite this improvement, so far presented versions of the setup for dispersion spectroscopy of liquids have reported lower sensitivity than absorption spectroscopy and the advantages of dispersion sensing at constant sensitivity yielding high linearity and extended dynamic ranges for chemical detection have not yet been fully evoked.

In this work, we present a refined version of the external-cavity QCL-based Mach-Zehnder interferometer setup for dispersion spectroscopy of liquid-phase samples, which features greater compactness and ability for fast acquisition at constant sensitivity. We describe the improvements in the instrumentation and investigate the influence of the miniaturization and the implementation of a fast hysteresis-free piezo-actuator for phase locked interferometric detection on the figures of merit (limits of detection) for dispersion sensing. In this context, we compare the performance of the refined setup with the previously demonstrated protype, by comparing the figures of merit for univariate glucose detection.

2. EXPERIMENTAL

The latest generation of the QCL-based Mach-Zehnder interferometer for broadband dispersion spectroscopy of liquid-phase samples is depicted in Figure 1A. A thermoelectrically cooled external-cavity quantum cascade laser (DRS Daylight Solutions Inc., San Diego, CA), tunable from 1230 to 890 cm^{-1}, was employed as IR light source and operated in a pulsed mode (100 kHz, 5% duty cycle). The laser beam is first guided by 0.5-inch mirrors towards the interferometer, formed by closely spaced 0.5-inch optical components. The overall dimensions of the free-space MZI are 70 x 8 mm. As the beam enters the MZI, it is split equally by a 50:50 ZnSe beam splitter (Thorlabs BSW705) and is further directed onto a new, miniaturized temperature stabilized dual-channel transmission cell (Figure 1B). The cell consists of two metal parts (front and back) milled from Aluminium (6082-T651) between which a pair of calcium fluoride (CaF_2) windows and a PTFE spacer are sandwiched. The 1-mm-thick rubbers are used as an interface between the metal parts and fragile CaF_2 windows. The cell features two liquid channels, cut out from a single PTFE spacer inserted between a pair of wedged 1 mm thick CaF_2 (25 x 15 mm) windows (Crystran Ltd., UK). After the cell, the two beams recombine at the second ZnSe beam splitter and are focused by parabolic mirrors at the two closely matched high-speed thermoelectrically (TE) cooled mercury cadmium telluride (MCT) detectors (PVI-4TE-10.6, Vigo Systems S.A., Poland; detectivity ≥2.0x10^9 cm $Hz^{1/2}$/W at 10.6 µm) mounted on a single post. The differential signal from the detectors is processed by a lock-in amplifier (MFLI, Zurich Instruments AG, Zurich, Switzerland) and digitized by a NI DAQ (NI-9205, National Instruments Corp.). Based on the differential signal, a piezo-actuator (P-841.1, Physik Instrumente, Germany; 2 ms settling time; 0.3 nm resolution) attached to one of the interferometric mirrors actively compensates for the relative phase shifts between the MZI arms induced by the sample during spectral scanning, enabling phase-locked interferometric detection at the quadrature point ($\pi/2$). The piezo-mirror displacement is controlled via PID control using the differential detector signal as the input for the lock-in amplifier. The displacement signal is proportional to refractive index changes of the sample, hence it is used as the analytical signal. With the setup, both absorption and dispersion spectra can be subsequently acquired, allowing internal comparison, and referencing via Kramers-Kronig calculations. For this purpose, an automated beam shutter for rapid and automatic switching between the two measuring modes was employed and synchronized via LabVIEW with the scan trigger of the laser. In addition, all optical components of the setup are housed and placed on a water-cooled breadboard (Thorlabs MBC3045/M) combined with a liquid cooling system (ThermoCube Liquid-to-Liquid, Solid State Cooling Systems) for enhanced temperature control and stabilization of the setup components and the internal environment.

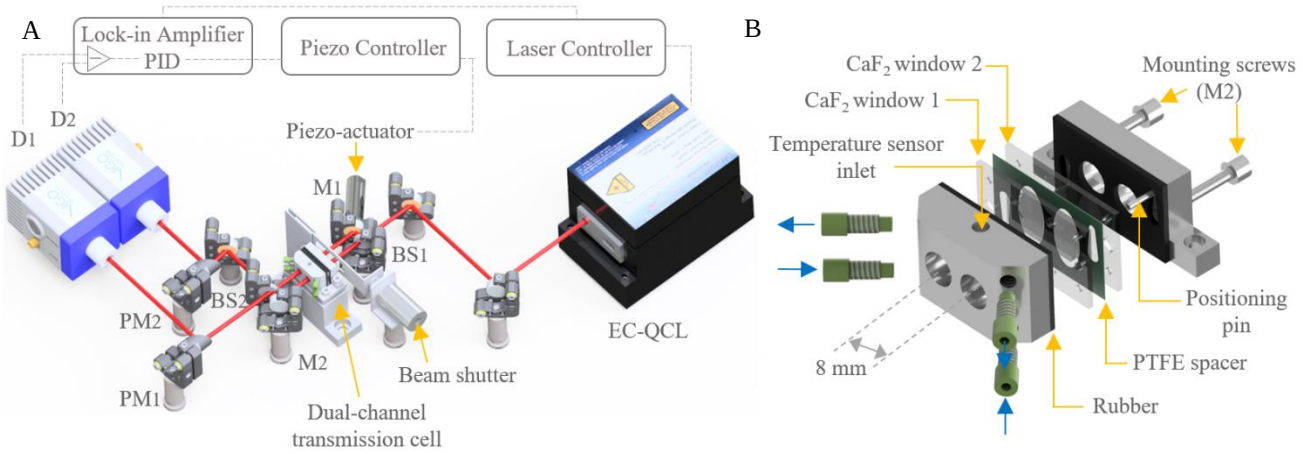

Figure 1. (A) Schematic of the latest generation experimental setup for dispersion spectroscopy of liquids. The MZI is composed of two mirrors (M_1, M_2) and two beam splitters (BS_1, BS_2). Two parabolic mirrors with different focal lengths are used to focus the IR beam onto the two MCT detectors (D_1, D_2). (B) A new miniaturized temperature-stabilized dual-channel transmission cell dedicated for the setup.

2.1 Spectra acquisition

Dispersion spectra were recorded with a laser tuning speed of 100 cm^{-1} s^{-1} by monitoring the displacement δ of the piezo-actuator needed to keep the interferometer in its quadrature point (difference signal = 0) using a controlled feedback loop. Figure 2 depicts the used measuring principle.[9,11] In general, the refractive index change Δn in the proximity of the absorption band leads to a change in the optical pathlength ΔL, which can be measured by an interferometer as a phase shift Δφ between the interfering waves.

A

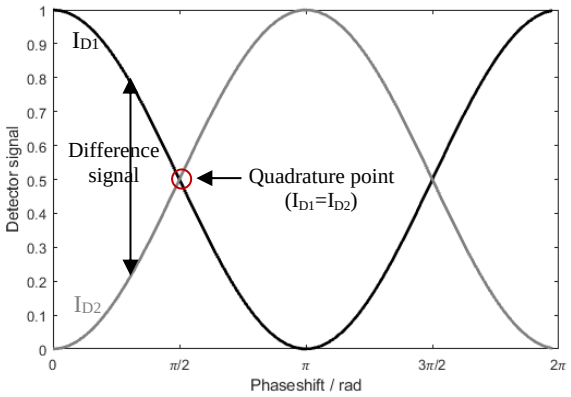

B

$$\boldsymbol{I_{D1}} = |E_r + E_s|^2 = I_r + I_s + 2\sqrt{I_r I_s}\cos(\Delta\boldsymbol{\varphi})$$

$$\boldsymbol{I_{D2}} = |E_r + E_s|^2 = I_r + I_s + 2\sqrt{I_r I_s}\cos(\Delta\boldsymbol{\varphi} + \pi)$$

$$\boldsymbol{I_{D1}} \sim \cos^2\left(\frac{\Delta\varphi}{2}\right) \qquad \boldsymbol{I_{D2}} \sim \sin^2\left(\frac{\Delta\boldsymbol{\varphi}}{2}\right)$$

$$\Delta\boldsymbol{\varphi}(\tilde{\nu}) = \frac{2\pi}{\lambda}\boldsymbol{\Delta L}(\tilde{\nu}) = \frac{2\pi}{\lambda}\boldsymbol{\Delta n}(\tilde{\nu}) \cdot d = \frac{2\pi}{\lambda}\boldsymbol{\delta}(\tilde{\nu}) \cdot \sqrt{2}$$

Figure 2. (A) Schematic representation of the intensity response of the two detectors (D_1, D_2) at varying phase shifts. At the quadrature point, the interferometer shows its highest sensitivity and stability. (B) Principles of Mach-Zehnder interferometry, where E_r and E_s, I_r and I_s are the electric fields and intensities in the reference and sample arm of the interferometer, respectively. I_{D1} and I_{D2} are the intensities of the interference pattern recorded at the detectors and their dependence on the phase shift Δφ.

Hence, the interference pattern provides the information about the phase shift, which is proportional to the change in the optical pathlength induced by the solutes present in the sample, and thus the refractive index changes of the solutes. The motion of the piezo-mirror is proportional to the optical pathlength and the refractive index spectrum of the solutes can be calculated, as follows:

$$\Delta n(\tilde{\nu}) = \frac{\Delta L(\tilde{\nu})}{d} = \frac{\delta(\tilde{\nu}) \cdot \sqrt{2}}{d} \quad (1)$$

where, the term $\delta \cdot \sqrt{2}$ stems from the physical displacement of the piezo-mirror along the diagonal line, and d is the geometrical pathlength (transmission pathlength). To obtain a refractive index sample, two measurements are performed for solvent vs. solvent (reference) and sample vs. solvent (sample) solutions and the recorded dispersion spectra are subtracted from each other.

Absorption spectra were recorded by blocking the beam in one of the interferometric arms with a movable shutter. The total amount of light transmitted through one flow cell filled with solution was measured by summing up the intensity recorded by the two detectors. Measurements were made for solvent I_0 and sample solutions I and the absorption spectrum was calculated as follows:

$$A(\tilde{\nu}) = -\log_{10}\left(\frac{I_{D1+D2}(\tilde{\nu})}{I_{0\,D1+D2}(\tilde{\nu})}\right) \quad (2)$$

2.2 Reagents and samples

Stock solution of D-(+)-Glucose (≥99.5%, Sigma-Aldrich) was prepared and diluted in ultrapure water (18 MΩ, Millipore, Bedford, USA) to five concentrations ranging from 2 to 10 g L^{-1}. Ethanol (96%, Sigma-Aldrich) was diluted in ultrapure water to eleven concentrations ranging from 1 to 50 v/v%.

3. RESULTS AND DISCUSSION

3.1 Experimental measures to improve the setup performance

The most compact (miniaturized) system of EC-QCL-based MZI setup was realized using free-space optics. The overall dimensions of the free-space configuration of the interferometer were significantly reduced from 200 x 50 mm presented in the previous version of the benchtop setup[9] to merely 70 x 8 mm by using 0.5-inch optics. This resulted in an almost 18-times reduction of the total area of the MZI. The new, close spacing between the interferometric arms (8 mm) yielded not only an easier alignment of the interferometer but also improved thermal and environmental stability and increased ruggedness of the new setup. Consequently, any change in the system, such as the exchange of the laser source or the removal of the transmission cell for a spacer exchange (e.g., to set up a new path length for transmission measurements), has minimal effect on the interferometer's alignment and can be easily performed.

Due to the reduced spacing between the interferometer arms (8 mm), a new miniaturized temperature-stabilized dual-channel sample fluidic cell was realized and employed (see Figure 1B). The overall size of the new cell was notably reduced, and the volume of the single sample compartment was decreased two-fold to 10 µL (for PTFE spacer of d=50 µm) and the minimum amount of sample needed for analysis including the inlet tubing (length of ~50 cm and $\emptyset_{ID}$ of 0.25 mm) is 24.5 µL. As the reference and the sample channels are defined by a common spacer inserted between one pair of windows, it helped to reduce the problematic inequalities between the transmission pathlengths in the two channels from ± 2 µm, presented in the previous version of the cell featuring two separate spacers and window pairs[9], to merely ± 0.2 µm. The achieved disproportion accounts for 0.126 rad (7.2°) for λ= 10 µm, which can be more easily compensated than the previous 72° (almost half of the wavelength). Moreover, such design is more resistant towards adverse effects induced by manual sample injection, during which fluctuating pressure might cause changes in the pathlength introducing drifts between spectra. In the new cell, every injection will affect both channels more uniformly. In general, it is beneficial, also temperature-wise, to manufacture fluidics dedicated for interferometric detection from common parts and materials.

To truly unlock the advantages of dispersion spectroscopy a new, faster, and hysteresis-free piezo-actuator was incorporated in the system and attached to one of the interferometric mirrors enabling a reliable, and repeatable acquisition at constant and high sensitivity. Incorporation of this component allowed to extend the dynamic range of the technique. The actuator holds the interferometer in the quadrature point throughout the measurement, while the built-in position sensor gives precise readout on the piezo-displacement in µm. This element has also enabled the increase in the acquisition speed from 1 cm^{-1} s^{-1} [(9)] to 100 cm^{-1} s^{-1}, hence the maximum tuning rate of the employed laser could be used, significantly reducing the spectra acquisition times from 5 min 30 sec. to 3.3 seconds and allowing spectral averaging (Figure 3A). Results presented in Figure 3A show that through scan averaging, the noise of the technique was minimized and reached ~1.84 x 10^{-5} [RIU] by averaging 10 scans. Additionally, long-term stability of the interferometric measurements was tested by continuous recording of baselines over time (> 4 hours). Figure 3B depicts the RMS noise levels, obtained by subtracting the first scan from the subsequent scans recorded over time. The results show that the deviations between baselines are

minimal and remain at the noise level corresponding to the value achieved by averaging one scan (see Figure 3A). Such behavior indicates high reproducibility of the recorded baseline in time, additionally confirming reproducibility in the piezo-element's motion. The system features stable operation in the entire time-window used for characterization and remains in the quadrature point of the interferometer, eliminating the need for fine adjustments before measurements.

Finally, the setup features thermal stabilization (water-cooled breadboard), which was already included before,[10] that separates the optomechanical components from the optical table made of aluminum and prevents adverse effects (drifts) of its thermal expansion on the interferometer alignment caused by the fluctuating temperature of the lab environment. Upon system miniaturization, the employed thermal control acts more effectively on the smaller setup. In addition, the new cell also features thermoelectric cooling (TEC) consisting of an NTC thermistor (slot in the top part of the cell) and a 15x15 mm Peltier element (underneath) with a TEC providing PID control. With this set of components, the temperature of the liquid inside the cell can be precisely and efficiently controlled (± 0.0007 °C at T=25 °C) and stably tuned between 15 to 80 °C, while keeping a low noise level, in terms of root-mean-square (RMS) values, for the refractive index change detection in the given temperature range (Figure 4). This opens the possibility for temperature dependent chemical reaction monitoring using dispersion spectroscopy.

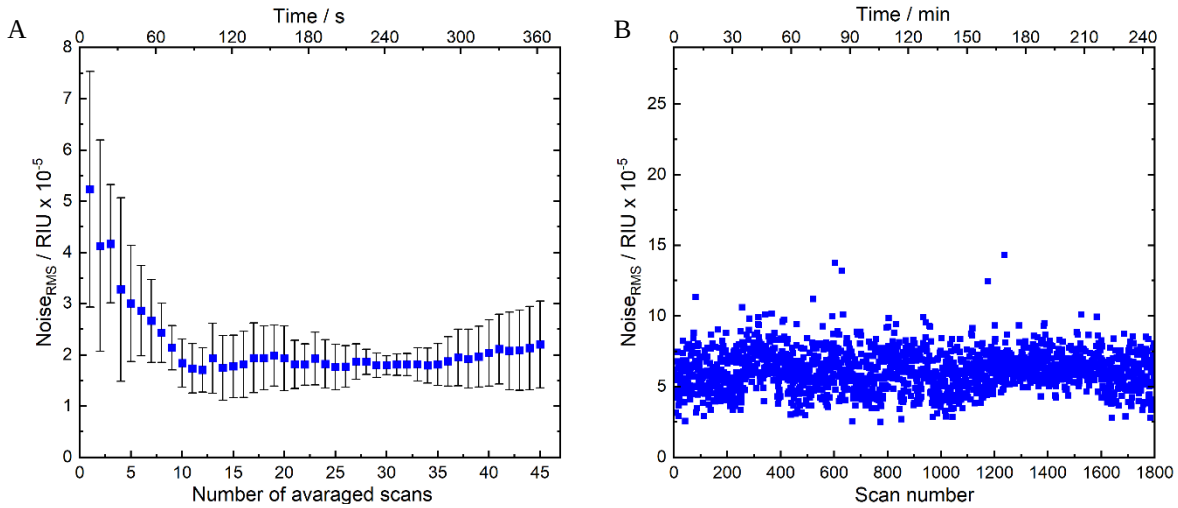

Figure 3. (A) RMS noise level for dispersion measurements calculated between 975 and 1175 cm^{-1} (average of 6 measurements) as a function of time and the total number of scans used for averaging. The lowest noise level of ~1.84 x 10^{-5} [RIU] was reached by averaging 10 scans, which corresponds to the total averaging time of ~65 seconds. After this time, the noise level remains stable. (B) RMS noise level of the baselines, obtained by subtracting the first scan from the subsequent scans recorded over time.

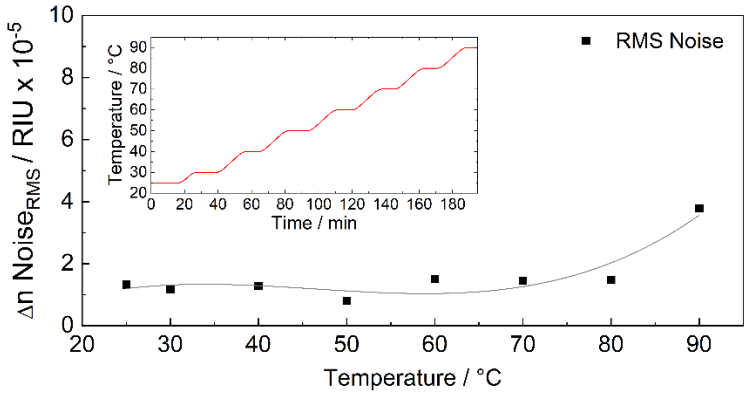

Figure 4. RMS noise level of dispersion spectroscopy as a function of the temperature of the cell. Gray solid line is added as a guide to the eye. (Inset) Temperature tuning range of the TEC control applied in the cell.

3.2 Comparison with the previous generation

To assess the impact of the applied optimization and miniaturization measures, the performance of the new setup was compared with the previous version of the setup reported and published in [9]. Table 1 describes the general components and differences between the setups under comparison. In the new version, the use of fast photon-sensitive MCT detectors, in combination with a much faster 'forward-sweep' tuning mode of the laser, enables rapid spectra acquisition. This significantly reduces the impact of low frequency noise (drifts) caused by external environmental factors. Compared to an earlier version of the benchtop setup, higher number of data points (~3000 points/spectrum) can be recorded in the forward-sweep mode yielding higher resolution spectra and coaddition of multiple scans for noise reduction as well as minor filtering of the acquired spectra.

Table 1. Comparison of the setup characteristics for the first and the latest generation benchtop EC-QCL-MZI setup.

Setup version	First generation[9]	Latest generation
Laser	EC-QCL (900-1230 cm^{-1})	EC-QCL (900-1230 cm^{-1})
Interferometer size / mm	200 x 50	70 x 8
Detector type	Pyroelectric	MCT
Thermal control	No	Yes (water-cooled breadboard)
Spectral acquisition	330 sec. / 1 scan (Step-and-measure)	3.3 sec. / 1 scan (Forward Sweep)

To evaluate the capabilities of the refined setup for quantification purposes, the new benchtop setup was used to record dispersion and absorption spectra of glucose diluted in water to concentrations ranging from 2 to 10 g L^{-1}. The pathlength used for transmission measurements was of 50 µm. The recorded spectra are presented in Figure 5. The investigated spectral region covers characteristic IR bands at 994, 1036, 1081, 1108 and 1153 cm^{-1}, which can be assigned to C-O stretching, C-C stretching as well as C-O-H bending modes of the glucose molecule.[12] Ten spectra were averaged per spectrum corresponding to 65 seconds of measuring time and filtered with Savitzky-Golay filter (order: 3, window 75 points/~8 cm^{-1}).

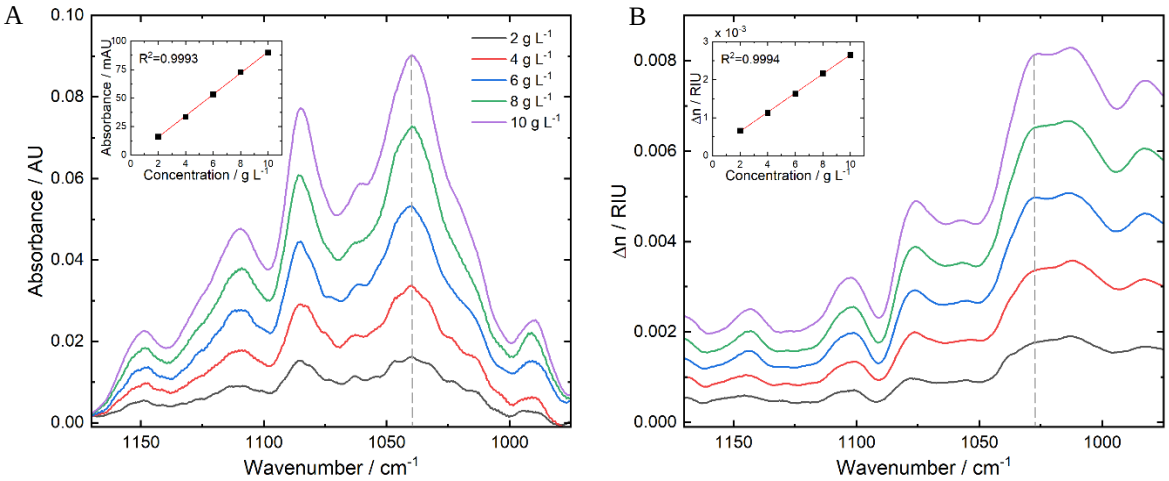

Figure 5. (A) Absorption spectra of glucose recorded with the miniaturized benchtop MZI setup. Inset shows the univariate calibration evaluated at 1036 cm^{-1}. (B) Dispersion spectra of glucose recorded with the miniaturized benchtop MZI setup. Inset shows univariate calibration by evaluation at the position of the beginning of anomalous dispersion corresponding to absorption band at 1036 cm^{-1}.

In the next step, the quantitative analysis on the recorded spectra was performed and the results can be found in Table 2. For quantitative analysis of the absorption spectra, the band height was evaluated at the most prominent IR band at 1036 cm^{-1}. The dispersion spectra were evaluated similarly, by assessing the maximum of the refractive index function change in the vicinity of the absorption band at 1036 cm^{-1}. With coefficients of determinations of >0.999, excellent calibration

could be achieved with both spectra acquisition methods (Figure 5 insets). The noise for both modalities was assessed by calculating root-mean-square (RMS) noise level in the spectral region of 975 – 1175 cm^{-1}. The limits of detection (LOD) were evaluated as $LOD = 3 \cdot Noise_{RMS}/Signal$, where signal is a slope of the calibration function.

Table 2. Comparison of the quantitative results obtained for dispersion and absorption spectroscopy using the first and the latest generation benchtop EC-QCL-MZI setup.

Setup version	First generation[9]		Latest generation	
Measuring mode	Absorption	Dispersion	Absorption	Dispersion
Measurement time	330 sec. / 1 scan		65 sec. / 10 scans	
Analyte	Glucose in H_2O		Glucose in H_2O	
Signal / AU/g L^{-1} / RIU/g L^{-1}	1.1 x 10^{-2}	4.1 x 10^{-4}	0.9 x 10^{-2}	5.6 x 10^{-4}
$Noise_{RMS}$ / AU / RIU	6.7 x 10^{-4}	7.3 x 10^{-5}	5.8 x 10^{-4}	1.8 x 10^{-5}
Limit of detection / g L^{-1}	0.19	0.53	0.19	0.10

It can be seen in Table 2, that the achieved LOD for absorption spectroscopy is comparable with the one obtained with a previous generation setup. This means, that the optimization measures had minor effect on the setup's LOD for classic absorption measurements, however this performance can be achieved at 5 times faster spectra acquisition time. As expected, bigger effect of the miniaturization and thermal stabilization can be observed on the interferometric-based dispersion sensing. For this modality, 5 times lower LOD was achieved when compared to the previous setup at 5 times lower spectra acquisition time. It is also the first report, showing that dispersion spectroscopy outperforms classic absorption spectroscopy for liquid-phase sensing, achieving nearly 2 times lower LOD for glucose detection.

4. CONCLUSION AND OUTLOOK

The next generation of the EC-QCL-based MZI setup for broadband dispersion spectroscopy of liquid-phase was realized. It features greater compactness and ability for fast acquisition at constant sensitivity. The employed balanced detection (analysis of difference signal of the detectors) offers the benefit that power fluctuation of the laser and common mode noise are highly rejected, reducing the noise of the technique. In summary, this modality benefits from miniaturization (outlook for on-chip MZI-based mid-IR sensor), thermal stabilization, and faster acquisition times. We increased the long-term stability and repeatability of the system enabling the possibility of time and temperature chemical reaction tracking with dispersion spectroscopy. Most importantly, this work demonstrated that dispersion spectroscopy can surpass classic absorption sensing.

ACKNOWLEDGEMENTS

This work has received funding from the European Union's Horizon 2020 research and innovation program under grant agreement no. 780240. A.S. acknowledges funding by the Austrian Science Fund FWF (project no. P32644-N).

REFERENCES

[1] Stuart, B., [Infrared spectroscopy: fundamentals and applications], John Wiley & Sons, Ltd (2004).
[2] Faist, J., Capasso, F., Sivco, D., Sirtori, C., Hutchinson, A. and Cho, A., "Quantum cascade laser," Science (80-.). **264**(April), 553–556 (1994).
[3] Schwaighofer, A. and Lendl, B., "Quantum cascade laser-based infrared transmission spectroscopy of proteins in solution," [Vibrational Spectroscopy in Protein Research], Elsevier, 59–88 (2020).
[4] Ramer, G. and Lendl, B., "Attenuated Total Reflection Fourier Transform Infrared Spectroscopy," Encycl. Anal. Chem. (2013).
[5] Nikodem, M. and Wysocki, G., "Molecular dispersion spectroscopy--new capabilities in laser chemical sensing.," Ann. N. Y. Acad. Sci. **1260**(1), 101–111 (2012).
[6] Wysocki, G. and Weidmann, D., "Molecular dispersion spectroscopy for chemical sensing using chirped mid-

infrared quantum cascade laser," Opt. Express **18**(25), 26123–26140 (2010).
[7] Martín-Mateos, P., Hayden, J., Acedo, P. and Lendl, B., "Heterodyne Phase-Sensitive Dispersion Spectroscopy in the Mid-Infrared with a Quantum Cascade Laser," Anal. Chem. **89**(11), 5916–5922 (2017).
[8] Hayden, J., Hugger, S., Fuchs, F. and Lendl, B., "A quantum cascade laser-based Mach–Zehnder interferometer for chemical sensing employing molecular absorption and dispersion," Appl. Phys. B **124**(2), 29 (2018).
[9] Lindner, S., Hayden, J., Schwaighofer, A., Wolflehner, T., Kristament, C., González-Cabrera, M., Zlabinger, S. and Lendl, B., "External Cavity Quantum Cascade Laser-Based Mid-Infrared Dispersion Spectroscopy for Qualitative and Quantitative Analysis of Liquid-Phase Samples.," Appl. Spectrosc. **74**(4), 452–459 (2020).
[10] Dabrowska, A., schwaighofer, A., Lindner, S. and Lendl, B., "Mid-IR Refractive Index Sensor for Detection of Proteins employing an External Cavity Quantum Cascade Laser-based Mach-Zehnder Interferometer," Opt. Express **28**(24), 36632–36642 (2020).
[11] Lendl, B., Schwaighofer, A., Kristament, C. and Montemurro, M., "A photothermal Mach-Zehnder interferometer for measuring caffeine and proteins in aqueous solutions using external cavity quantum cascade lasers," 19 (2018).
[12] Kačuráková, M. and Mathlouthi, M., "FTIR and laser-Raman spectra of oligosaccharides in water: characterization of the glycosidic bond," Carbohydr. Res. **284**(2), 145–157 (1996).

*bernhard.lendl@tuwien.ac.at; phone +43/1/58801-15140; fax +43/1/58801-15199; http://www.cta.tuwien.ac.at/cavs/